JACS
JOURNAL OF THE AMERICAN CHEMICAL SOCIETY

Communication

pubs.acs.org/JACS

Direct Light-Driven Water Oxidation by a Ladder-Type Conjugated Polymer Photoanode

Pauline Bornoz, Mathieu S. Prévot, Xiaoyun Yu, Néstor Guijarro, and Kevin Sivula*

Laboratory for Molecular Engineering of Optoelectronic Nanomaterials, École Polytechnique Fédérale de Lausanne (EPFL), Station 6, 1015 Lausanne, Switzerland

Supporting Information

ABSTRACT: A conjugated polymer known for high stability (poly[benzimidazobenzophenanthroline], coded as BBL) is examined as a photoanode for direct solar water oxidation. In aqueous electrolyte with a sacrificial hole acceptor (SO_3^{2-}), photoelectrodes show a morphology-dependent performance. Films prepared by a dispersion-spray method with a nanostructured surface (feature size of ~20 nm) gave photocurrents up to 0.23 ± 0.02 mA cm^{-2} at 1.23 V_{RHE} under standard simulated solar illumination. Electrochemical impedance spectroscopy reveals a constant flat-band potential over a wide pH range at +0.31 V_{NHE}. The solar water oxidation photocurrent with bare BBL electrodes is found to increase with increasing pH, and no evidence of semiconductor oxidation was observed over a 30 min testing time. Characterization of the photo-oxidation reaction suggests H_2O_2 or •OH production with the bare film, while functionalization of the interface with 1 nm of TiO_2 followed by a nickel−cobalt catalyst gave solar photocurrents of 20−30 μA cm^{-2}, corresponding with O_2 evolution. Limitations to photocurrent production are discussed.

Photoelectrochemical (PEC) cells have long held promise as an inexpensive route for the storage of solar energy as chemical bonds.[1] A dual band gap tandem cell with an n-type semiconductor photoanode connected in series to a p-type photocathode can split water into O_2 and H_2 at a solar-to-hydrogen (STH) efficiency potentially over 20% even assuming reasonable losses.[2] However, economically competitive PEC H_2 production at a scale commensurate with the global energy demand requires not only high efficiency but also long-term stability and the ability to construct large-area devices at a fraction of the cost of traditional high-performance semiconductor devices.[3] While many promising semiconducting materials are currently under development, the identification of new robust photoelectrode materials with ideal energy levels and inexpensive production is urgently needed.

One class of semiconductors that offers tunable energy levels and processability in many solvents is the π-conjugated organic polymers. While their promising aspects have motivated intense investigation for economical roll-to-roll organic photovoltaic (OPV) devices, due to their poor stability in aqueous conditions, they have not been generally pursued as photoelectrodes for direct solar water splitting.[4] Encapsulated OPVs have recently been demonstrated in PV-biased photoelectosynthetic cells for solar water splitting,[5] but the lack of intrinsic material stability limits their application in this configuration. Polymeric carbon nitride based materials[6] and conjugated microporous network polymers[7] have recently shown promising performance for the direct solar water reduction, suggesting that conjugated carbon-based materials can be suitable as photocathodes. However, the task of identifying suitable π-conjugated materials for the photoanode is more difficult due to the harsh conditions of photoelectrochemical water oxidation. Organic dyes based on porphyrins or perylene diimides (PDIs) can possess HOMO levels suitable for water oxidation in certain conditions.[8−10] However, solution-processing these materials can be problematic given their strong tendency to aggregate.[11] As certain conjugated polymers can possess similar energy levels to porphyrin and PDI dyes while also exhibiting superior film forming characteristics and improved intrinsic stability, we hypothesized that they could be viable candidates for inexpensive solution-processed photoanodes.

Here we present promising performance and stability of an n-type polymer, poly(benzimidazobenzophenanthroline), known as BBL, as a photoanode in a direct semiconductor-liquid junction (SCLJ) configuration for solar water oxidation. Indeed, among n-type conjugated polymers BBL is a ladder-type polymer known for exceptional stability[12] and good electron mobility up to 0.1 $cm^2\ V^{-1}\ s^{-1}$.[13] BBL has been reported as an electron acceptor in OPV cells,[14] as a buffer layer for inorganic thin-film PV,[15] and for n-channel field-effect transistors.[16] These favorable aspects encouraged us to consider BBL for PEC application.

To begin our investigation of BBL as a potential photoanode material, we first examined the effect of the thin-film morphology on the extraction of photogenerated charges. Indeed, the relatively short excited-state transport length expected in BBL[17] suggests a high surface area mesostructured SCLJ would be beneficial to charge extraction similar to a bulk heterojunction OPV. BBL thin-films were prepared via two different deposition techniques: dip coating from a BBL solution in methanesulfonic acid (MSA)[19] and spray deposition of an aqueous BBL nanofiber dispersion.[18,20] See Supporting Information for full details of the thin-film formation methods.

Scanning electron microscopy (SEM, Figure 1) reveals considerable morphological differences with respect to the deposition technique. While both films display a homogeneous coverage of the FTO, the dip-coated film (Figure 1a) shows a

Received: June 10, 2015
Published: November 18, 2015

DOI: 10.1021/jacs.5b05724
J. Am. Chem. Soc. 2015, 137, 15338−15341

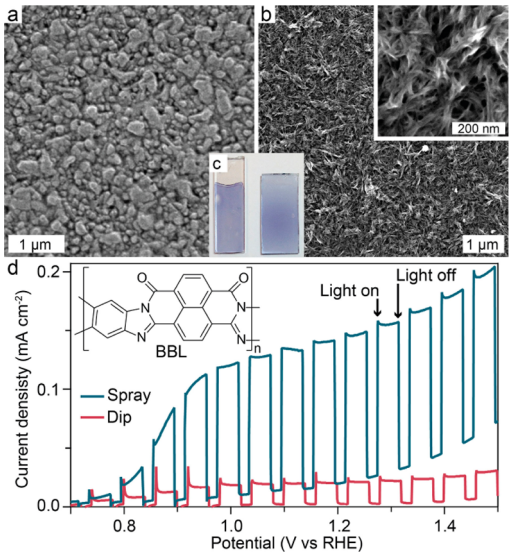

Figure 1. SEM top view of an optimized dip-coated (a) and sprayed (b) films with optical images of both electrodes (c). Panel (d) shows the *J*–*V* curve of a thin sprayed film (blue line) and a dip-coated film (red line) in sacrificial electrolyte (0.5 M Na_2SO_3, pH 7) under chopped light substrate-side illumination (scan rate 10 mV s^{-1}).

relatively smooth surface with feature size similar to the underlying FTO (100–500 nm, see additional SEM images in Figure S1). In contrast, the spray-coated film (Figure 1b) exhibits feature size as small as 20 nm and a higher roughness due to the interconnecting network formed from the nanofiber dispersion.

To determine the effect of the morphology on the PEC performance we prepared films using both deposition methods to have similar light absorption (Figure 1c). The absorptance spectra (Figure S2) reveal a maximum of ∼40% light absorption at λ = 590 nm, corresponding to an average thickness of 40 nm based on the reported absorption coefficient.[21] A Tauc plot analysis verified a direct band gap transition at 1.86 eV matching previously reported values.[13] We note that preparing thicker films by dip coating was not possible given solubility limitations. The two similarly absorbing films were next examined by linear scanning voltammetry (LSV) in a three-electrode PEC cell using a buffered aqueous electrolyte (pH 7) and a hole scavenger (SO_3^{2-}) under intermittent simulated solar illumination (100 mW cm^{-2}). The oxidation of SO_3^{2-} is thermodynamically and kinetically more facile than the oxidation of water.[22] As such, measuring photocurrent for SO_3^{2-} oxidation enables the investigation of the PEC properties of BBL with minimum kinetic limitations. The LSV data are presented in Figure 1d with respect to the reversible hydrogen electrode (RHE). Both BBL electrodes show an anodic photocurrent upon illumination (n-type behavior) and reproducibility in the potential range scanned. Moreover, the LSV behavior offers insight into charge transport and transfer. The dip-coated film exhibits transient spikes when illuminated in the photocurrent onset range (from +0.7 to 1.0 V_{RHE}), suggesting a limitation of charge transfer to the SO_3^{2-} (accumulation of holes at the SCLJ). In contrast, only small spikes are seen in the spray-coated film, and the photocurrent density in the plateau region (from +1.0–1.3 V_{RHE}) is 6.5 times higher. Given the similar light absorption of the two electrodes, it is reasonable to conclude that greater photocurrent density of the spray-coated film results from the porous morphology, which facilitates harvesting of the photo-excited states due to their short transport distance.

Optimization of the spray-coating deposition method showed that films thicker than 40 nm gave higher photocurrent density, J_{ph}, (Figure S3). Electrodes with a thickness of about 120 nm gave an average J_{ph} of 0.23 ± 0.02 mA cm^{-2} at +1.23 V_{RHE}, while thicker films gave lower values. J_{ph} was consistently ∼30% larger for substrate-side illumination (compared to electrolyte-side) indicating a limitation in majority carrier (electron) transport. This observation together with the effect of the nanostructure are consistent with free charge generation occurring exclusively in high proximity to the SCLJ, where excitons are split either by direct hole injection into the electrolyte or a space-charge electric field. The electron transport could be perhaps limited due to grain boundaries between the individual fibers.

To next obtain information regarding the electronic structure of the SCLJ and determine the suitability of BBL to oxidize water, electrochemical impedance spectroscopy and Mott–Schottky (M–S) analysis were performed on spray-coated electrodes at various pH without sacrificial hole acceptors. We used thicker films (230 nm) to avoid direct substrate–electrolyte contact. Figure 2a shows the M–S plot obtained using the space charge

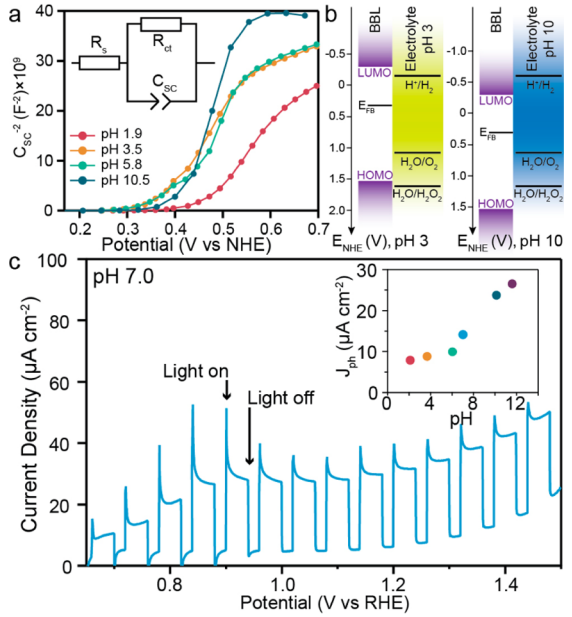

Figure 2. (a) Mott–Schottky plot from a sprayed-deposited BBL film in aqueous electrolyte (buffered sulfate/phosphate) at various pH. A Randle equivalent circuit was used to fit the impedance data (inset). (b) Energy band diagram of BBL under flat-band condition at pH 3 and 10. (c) *J*–*V* (LSV, 10 mV s^{-1}) curve in aqueous sulfate/phosphate electrolyte (pH 7) under chopped illumination. The inset shows the evolution of the photocurrent density at 1.23 V_{RHE} with the pH.

capacitance, C_{sc}, extracted from the Nyquist plots (Figure S4), which were fit with a simple Randle equivalent circuit (Figure 2a inset). For each pH, the expected accumulation region, where C_{sc}^{-2} is small, is observed in Figure 2a at potentials <∼ +0.25 V vs the normal hydrogen electrode (V_{NHE}). At more positive voltages, an increase in C_{sc}^{-2} is observed consistent with a space-charge depletion region. Complete depletion of the semiconductor film leads to a leveling-off of C_{sc}^{-2} at higher applied potentials. We note that application of the M–S model rigorously requires a planar electrode. The sublinear onset of the depletion region is reasonably due to a changing effective surface area as the small features of the electrodes are depleted.[23] Given the nanostructure, the flat band potential, E_{FB}, will be

DOI: 10.1021/jacs.5b05724
J. Am. Chem. Soc. 2015, 137, 15338–15341

overestimated by extrapolating the linear region of the plots, and thus E_{FB} is better estimated by regression of the onset region of C_{sc}^{-2}. Nevertheless, it is clear that in the pH range from 3.5 to 10.5, E_{FB} only varies slightly with pH. We estimate a value for E_{FB} of +0.31 ± 0.03 V_{NHE}, which is consistent with the observed onset of photocurrent when using the sacrificial hole acceptor SO_3^{2-}. In contrast, at pH 1.9 a positive shift of E_{FB} to +0.40 V is observed. While inorganic oxide semiconductors typically exhibit a Nernstian shift with pH due to the dynamic equilibrium of H^+ and OH^- adsorption/desorption,[24] it is likely that few (if any) species adsorb at the BBL/electrolyte interface in the pH range from 3.5 to 10.5 leading to the constant E_{FB}. In contrast, the known acido-basic behavior of BBL with a pK_a of 2.2[25] could explain the shift of E_{FB} at pH 1.9.

The E_{FB} estimation together with the band gap and LUMO position[13] allow construction of an energy band diagram of BBL in water at flat-band conditions for different pH (Figure 2b). At pH 3 the HOMO is well-positioned for the oxygen evolution reaction (OER), and the driving force for the OER reasonably increases with pH given the constant E_{FB} of the BBL. To evaluate the ability of the bare BBL to directly photo-oxidize water, we next measured 230 nm-thick spray-coated electrodes in aqueous electrolyte without a sacrificial hole scavenger at different pH. An example of a LSV at pH 7 is given in Figure 2c. Here the onset of photocurrent is similar to the sacrificial case, however the photocurrent density is considerably smaller and large transient spikes are observed, especially near the photocurrent onset potential. Remarkably, sustained photocurrent was observed as a plateau region of the LSV from ~ +0.9−1.4 V. The sustained J_{ph} in the plateau region (after the decay of the transient, taken to be 15 s, see Figure S5) under continuous 1 sun illumination (100 mW cm^{-2}) in different pH is given in the inset of Figure 2c. The magnitude of J_{ph} increases with pH consistent with the increasing driving force.

Importantly, the possibility that the photocurrent arises from oxidation of the BBL itself was eliminated through longer stability measurements (Figures S6 and S7). See full discussion in the Supporting Information.

The incident photon-to-current spectrum (IPCE, Figure S8) verifies that the photocurrent in nonsacrificial electrolyte at pH 7 arises from light absorption by the BBL. However, the observed reduction of the IPCE when using a white light bias can be ascribed to increased geminate recombination in the film,[26] and brings into question the nature of the sustained oxidation reaction occurring on the bare electrode (see Supporting Information for full explanation). In fact the observation of O_2 production by gas chromatography was unsuccessful despite that the expected concentration was within GC detection limits. This suggests that molecular O_2 is not the product of the sustained photo-oxidation reaction. Another possibility is that water oxidation occurs via a two-electron process producing H_2O_2. This oxidation is thermodynamically feasible (E = +1.8 V_{RHE}),[27] as it corresponds roughly to the estimated HOMO level position under flat band conditions at pH 6. Moreover ketonic functional groups on BBL could support the production of H_2O_2 similar to observations on oxidized carbon nanotubes.[28] However, H_2O_2 was not directly detectable in the electrolyte using titration with $KMnO_4$, likely because the produced H_2O_2 is directly reduced at the anode to produce the hydroxyl radical (•OH).[29] The occurrence of this pathway can be detected by using a florescence probe technique,[29,30] wherein coumarin reacts with hydroxyl radicals to produce a new compound (umbelliferone, see Figure 3a) quantifiable by photoluminescence spectroscopy. To

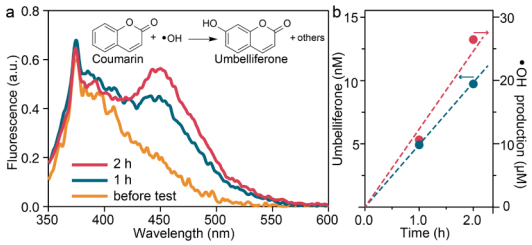

Figure 3. (a) The fluorescence probe reaction used to detect hydroxyl radicals (top) is shown together with the fluorescence spectra of buffered sulfate/phosphate aqueous electrolyte (pH 7) containing 0.1 mM coumarin (before test) and after the photoelectrochemical experiment at 1.23 V vs RHE for 1 and 2 h. (b) Comparison of the hydroxyl radical concentration estimated by the fluorescence probe to the calculated concentration from the photocurrent density.

demonstrate the production of the hydroxyl radical by BBL, a solution of coumarin (Figure S9) was used as described in the Supporting Information.

The photoluminescence spectra of the original electrolyte and after one or 2 h under photoelectrochemical operation with BBL are shown in Figure 3a, where peaks for coumarin at 374 nm and for umbelliferone at 450 nm are observed. The concentration of the umbelliferone in the electrolyte was estimated using a calibration curve (Figure S10) and is compared to the maximum amount of •OH that could have been produced (based on the integrated J_{ph}, and assuming 100% Faradaic efficiency) in Figure 3b. While the concentrations differ in magnitude significantly due to the low expected yield of the coumarin reaction[29] and other potential factors decreasing the umbelliferone production,[31] the rate of increase in the concentrations indicates a direct linear relation suggesting that the production of umbelliferone is correlated to the photocurrent and supporting the notion that the bare BBL produces the hydroxyl radical through photo-oxidation. Other possible routes for the production of •OH are discussed in the Supporting Information. Regardless of the origin of the •OH, its production—instead of molecular O_2 via the four-electron OER—is consistent with the lack of defined catalytic center on the bare BBL.

Given the demonstrated photoelectrochemical stability of the bare BBL photoanode and the thermodynamic suitability for water oxidation we next sought to show O_2 production by applying an appropriate co-catalyst overlayer. Attempts to directly attach an OER catalyst to the BBL surface did not result in sustained O_2 production, likely due to poor semiconductor/catalyst attachment. However, when the BBL was pretreated with a sufficiently thin layer of TiO_2 (~1 nm) to act as a tunnel junction, a suitable surface could be obtained (Figure S11) that allowed successful attachment of a nickel−cobalt catalyst.[32] LSV data are shown in Figure S12 for the film before and after the TiO_2 and with the co-catalyst. Application of the TiO_2 did not significantly change the observed J_{ph} (~15−20 μA cm^{-2}), however a slight increase (to ~30 μA cm^{-2}) was observed upon the application of the co-catalyst layer. Photocurrent transient spikes remain at all conditions. Despite this, gas chromatography confirmed molecular O_2 production at a rate of 20 ± 3 nmol h^{-1} during a constant-illumination chronoamperometry measurement when a steady-state J_{ph} of 10.3 ± 0.1 μA cm^{-2} was produced corresponding to a Faradaic efficiency of 82 ± 16% (similar to the value obtained with a related system).[10] Overall the similar onset behavior and J_{ph} observed with the overlayer present, compared to the bare film in sacrificial and nonsacrificial electrolytes,

DOI: 10.1021/jacs.5b05724
J. Am. Chem. Soc. 2015, 137, 15338−15341

suggest that charge separation in the semiconductor layer is kinetically limited by interfacial exciton dissociation[33] and thus ultimately controlled by the driving force as previously discussed. The use of a solid-state semiconductor heterojunction or other overlayers specifically designed to enhance free charge generation is a reasonable strategy to increase the photocurrent in BBL electrodes, and efforts in this direction are underway in our laboratory.

In summary, our investigations of BBL as a photoanode for solar water oxidation reveal a strong dependence of the sacrificial photocurrent density on the morphology of the film consistent with a limitation in excited-state transport to the SCLJ. Electrochemical impedance spectroscopy showed that the driving force for water oxidation could be tuned with electrolyte pH and suggested that water oxidation is thermodynamically feasible. Furthermore, for the first time, a π-conjugated organic semiconductor demonstrated sustained direct solar water oxidation. The water oxidation photocurrent density was found to increase with increasing pH, and no evidence of semiconductor oxidation was found over testing time on the order of hours with bare BBL films. H_2O_2 or hydroxyl radical production proceeds, instead of molecular O_2 evolution, on bare BBL likely due to the lack of catalytic sites. Notably the produced •OH could be employed to degrade organic pollutants in wastewater.[34] While molecular O_2 evolution was measured upon functionalization with a Ni−Co catalyst, the smaller photocurrents observed for water oxidation, compared to the sacrificial case, suggest a limitation in charge separation, which is related to the driving force for charge injection into the electrolyte. Overall this demonstration suggests that robust n-type conjugated organic semiconductors are suitable for direct PEC water oxidation and opens a new path for the rational design and optimization of photoanodes for solar water splitting.

■ ASSOCIATED CONTENT

Supporting Information

The Supporting Information is available free of charge on the ACS Publications website at DOI: 10.1021/jacs.5b05724.

Experimental details and data; figures S1−S12 (PDF)

■ AUTHOR INFORMATION

Corresponding Author

*kevin.sivula@epfl.ch

Notes

The authors declare no competing financial interest.

■ ACKNOWLEDGMENTS

We thank the Swiss national science foundation (project no. 200021_149251) and the European research commission (project CEMOS_336506) for financial support.

■ REFERENCES

(1) Walter, M. G.; Warren, E. L.; McKone, J. R.; Boettcher, S. W.; Mi, Q. X.; Santori, E. A.; Lewis, N. S. *Chem. Rev.* **2010**, *110*, 6446.

(2) (a) Seitz, L. C.; Chen, Z.; Forman, A. J.; Pinaud, B. A.; Benck, J. D.; Jaramillo, T. F. *ChemSusChem* **2014**, *7*, 1372. (b) Prevot, M. S.; Sivula, K. *J. Phys. Chem. C* **2013**, *117*, 17879.

(3) Pinaud, B. A.; Benck, J. D.; Seitz, L. C.; Forman, A. J.; Chen, Z.; Deutsch, T. G.; James, B. D.; Baum, K. N.; Baum, G. N.; Ardo, S.; Wang, H.; Miller, E.; Jaramillo, T. F. *Energy Environ. Sci.* **2013**, *6*, 1983.

(4) Yanagida, S.; Kabumoto, A.; Mizumoto, K.; Pac, C.; Yoshino, K. *J. Chem. Soc., Chem. Commun.* **1985**, *8*, 474.

(5) (a) Abe, T.; Tobinai, S.; Taira, N.; Chiba, J.; Itoh, T.; Nagai, K. *J. Phys. Chem. C* **2011**, *115*, 7701. (b) Bourgeteau, T.; Tondelier, D.; Geffroy, B.; Brisse, R.; Laberty-Robert, C.; Campidelli, S.; de Bettignies, R.; Artero, V.; Palacin, S.; Jousselme, B. *Energy Environ. Sci.* **2013**, *6*, 2706. (c) Guerrero, A.; Haro, M.; Bellani, S.; Antognazza, M. R.; Meda, L.; Gimenez, S.; Bisquert, J. *Energy Environ. Sci.* **2014**, *7*, 3666.

(6) Wang, X. C.; Maeda, K.; Thomas, A.; Takanabe, K.; Xin, G.; Carlsson, J. M.; Domen, K.; Antonietti, M. *Nat. Mater.* **2009**, *8*, 76.

(7) Sprick, R. S.; Jiang, J.-X.; Bonillo, B.; Ren, S.; Ratvijitvech, T.; Guiglion, P.; Zwijnenburg, M. A.; Adams, D. J.; Cooper, A. I. *J. Am. Chem. Soc.* **2015**, *137*, 3265.

(8) (a) Swierk, J. R.; Méndez-Hernández, D. D.; McCool, N. S.; Liddell, P.; Terazono, Y.; Pahk, I.; Tomlin, J. J.; Oster, N. V.; Moore, T. A.; Moore, A. L.; Gust, D.; Mallouk, T. E. *Proc. Natl. Acad. Sci. U. S. A.* **2015**, *112*, 1681. (b) Yu, Z.; Li, F.; Sun, L. *Energy Environ. Sci.* **2015**, *8*, 760.

(9) Youngblood, W. J.; Lee, S. H. A.; Kobayashi, Y.; Hernandez-Pagan, E. A.; Hoertz, P. G.; Moore, T. A.; Moore, A. L.; Gust, D.; Mallouk, T. E. *J. Am. Chem. Soc.* **2009**, *131*, 926.

(10) Kirner, J. T.; Stracke, J. J.; Gregg, B. A.; Finke, R. G. *ACS Appl. Mater. Interfaces* **2014**, *6*, 13367.

(11) Singh, R.; Giussani, E.; Mróz, M. M.; Di Fonzo, F.; Fazzi, D.; Cabanillas-González, J.; Oldridge, L.; Vaenas, N.; Kontos, A. G.; Falaras, P.; Grimsdale, A. C.; Jacob, J.; Müllen, K.; Keivanidis, P. E. *Org. Electron.* **2014**, *15*, 1347.

(12) Arnold, F. E.; Vandeuse, R. L. *Macromolecules* **1969**, *2*, 497.

(13) Babel, A.; Jenekhe, S. A. *J. Am. Chem. Soc.* **2003**, *125*, 13656.

(14) (a) Alam, M. M.; Jenekhe, S. A. *Chem. Mater.* **2004**, *16*, 4647. (b) Jenekhe, S. A.; Yi, S. J. *Appl. Phys. Lett.* **2000**, *77*, 2635.

(15) Gowrishankar, V.; Luscombe, C. K.; McGehee, M. D.; Frechet, J. M. J. *Sol. Energy Mater. Sol. Cells* **2007**, *91*, 807.

(16) (a) Babel, A.; Jenekhe, S. A. *J. Phys. Chem. B* **2002**, *106*, 6129. (b) Babel, A.; Jenekhe, S. A. *Adv. Mater.* **2002**, *14*, 371.

(17) Lin, J. D. A.; Mikhnenko, O. V.; Chen, J.; Masri, Z.; Ruseckas, A.; Mikhailovsky, A.; Raab, R. P.; Liu, J.; Blom, P. W. M.; Loi, M. A.; Garcia-Cervera, C. J.; Samuel, I. D. W.; Nguyen, T.-Q. *Mater. Horiz.* **2014**, *1*, 280.

(18) Janietz, S.; Sainova, D. *Macromol. Rapid Commun.* **2006**, *27*, 943.

(19) Jenekhe, S. A.; Johnson, P. O. *Macromolecules* **1990**, *23*, 4419.

(20) Briseno, A. L.; Mannsfeld, S. C. B.; Shamberger, P. J.; Ohuchi, F. S.; Bao, Z. N.; Jenekhe, S. A.; Xia, Y. N. *Chem. Mater.* **2008**, *20*, 4712.

(21) Osaheni, J. A.; Jenekhe, S. A.; Burns, A.; Du, G.; Joo, J.; Wang, Z.; Epstein, A. J.; Wang, C. S. *Macromolecules* **1992**, *25*, 5828.

(22) Stanbury, D. M. *Advances in Inorganic Chemistry*; Sykes, A. G., Ed.; Academic Press, Inc.: San Diego, CA, 1989; Vol 33, p 70.

(23) Mora-Seró, I.; Fabregat-Santiago, F.; Denier, B.; Bisquert, J.; Tena-Zaera, R.; Elias, J.; Lévy-Clément, C. *Appl. Phys. Lett.* **2006**, *89*, 203117.

(24) (a) Bolts, J. M.; Wrighton, M. S. *J. Phys. Chem.* **1976**, *80*, 2641. (b) Butler, M. A.; Ginley, D. S. *J. Electrochem. Soc.* **1978**, *125*, 228.

(25) (a) Wilbourn, K.; Murray, R. W. *Macromolecules* **1988**, *21*, 89. (b) Wilbourn, K.; Murray, R. W. *J. Phys. Chem.* **1988**, *92*, 3642.

(26) Brenner, T. J. K.; Vaynzof, Y.; Li, Z.; Kabra, D.; Friend, R. H.; McNeill, C. R. *J. Phys. D: Appl. Phys.* **2012**, *45*, 415101.

(27) Ando, Y.; Tanaka, T. *Int. J. Hydrogen Energy* **2004**, *29*, 1349.

(28) Lu, X.; Yim, W.-L.; Suryanto, B. H. R.; Zhao, C. *J. Am. Chem. Soc.* **2015**, *137*, 2901.

(29) Ohguri, N.; Nosaka, A. Y.; Nosaka, Y. *Electrochem. Solid-State Lett.* **2009**, *12*, B94.

(30) Zhang, J.; Nosaka, Y. *J. Phys. Chem. C* **2013**, *117*, 1383.

(31) Nakabayashi, Y.; Nosaka, Y. *J. Phys. Chem. C* **2013**, *117*, 23832.

(32) Trotochaud, L.; Ranney, J. K.; Williams, K. N.; Boettcher, S. W. *J. Am. Chem. Soc.* **2012**, *134*, 17253.

(33) Gregg, B. A.; Kim, Y. I. *J. Phys. Chem.* **1994**, *98*, 2412.

(34) Malato, S.; Fernández-Ibáñez, P.; Maldonado, M. I.; Blanco, J.; Gernjak, W. *Catal. Today* **2009**, *147*, 1.

DOI: 10.1021/jacs.5b05724
J. Am. Chem. Soc. 2015, 137, 15338−15341